

Large-Eddy Simulation of Interactions between a Reacting Jet and Evaporating Droplets

Jun Xia***, Kai H. Luo*, Suresh Kumar**

* School of Engineering Sciences, University of Southampton, Highfield, Southampton SO17 1BJ, UK

** FRS, BRE, Garston, Watford WD25 9XX, UK

ABSTRACT

Large-eddy simulation of a turbulent reactive jet with evaporating liquid droplets is performed to investigate the interactions among turbulence, combustion, heat transfer and evaporation. A hybrid Eulerian-Lagrangian approach is used for the gas-liquid flow system. Arrhenius-type finite-rate chemistry is employed for the chemical reaction. To capture the highly local interactions, dynamic procedures are used for all the subgrid-scale models, except that the filtered reaction rate is modelled by a scale similarity model. Various representative cases with different initial droplet sizes (St_0) and mass loading ratios (MLR) have been simulated, along with a reacting case without droplets. It is found that compared with the bigger, slow responding droplets ($St_0=16$), smaller droplets ($St_0=1$) are more efficient in suppressing combustion due to their preferential concentration in the reaction zones. The peak temperature and intensity of temperature fluctuation are found to be reduced in all the droplet cases, to a varying extent depending on the droplet properties. However, both the vorticity magnitude and turbulent kinetic energy may be enhanced where droplets reduce the local temperature and consequently the viscous dissipation. From the budget analysis of grid-scale kinetic energy (GSKE), it was found that the droplet evaporation effect on GSKE is small, while the droplet momentum effect greatly depends on St_0 . When the MLR is sufficiently high, the bigger ($St_0=16$) droplets can have profound influence on GSKE, and consequently on the formation and evolution of large-scale flow structures, entrainment and turbulent mixing.

INTRODUCTION

Multiphase reactive flows appear in many engineering applications, such as water/steam diluted gas turbine combustors and fire suppression systems, in which complex unsteady interactions exist among vortex dynamics, entrainment, mixing, turbulence, combustion and evaporating droplets at vastly disparate scales. The problem is also scientifically interesting and computationally challenging. Nevertheless, a systematic understanding of such multiscale, multiphysics systems is still far from being achieved. Fundamental numerical studies in the past usually adopted an idealized homogeneous [1, 2] or two-dimensional [3] flow in the laminar and transitional regimes. For spatially evolving flows, the gas-solid non-reactive isothermal jet has been investigated extensively with numerical and experimental techniques [4, 5], with a focus on particle effects on gas-flow turbulence, i.e., turbulence modulation. With the addition of chemical reaction and phase change, very few reported work can be found. Recently, Direct Numerical Simulation (DNS) of a spatially developing reactive planar mixing layer has been performed to study the effects of fine solid particles on flow turbulence with the assumption of no temperature variation [6]. The effects of turbulence on vaporization, mixing and combustion of liquid-fuel sprays were investigated by the Reynolds Averaged Navier-Stokes (RANS) approach in [7]. Compared with DNS and RANS, Large-Eddy Simulation (LES) is an ideal compromise between computational cost and numerical accuracy, which is being developed for reacting [8] and multiphase [9] flow simulations.

In the present study, a three-dimensional (3D) turbulent reactive jet laden with non-reactive evaporating liquid droplets has been simulated using LES. The LES ap-

proach uses the dynamic procedure to obtain six subgrid model coefficients in order to capture the highly local interactions among turbulence, combustion, heat transfer and evaporation. The complex interactions are then investigated under various representative conditions.

MATHEMATICAL MODELS AND NUMERICAL PROCEDURE

The flow field is described with the compressible time-dependent Navier-Stokes equations [10]. An idealized one-step irreversible reaction with the Arrhenius finite-rate chemistry is employed [10]. The subgrid scale (SGS) terms in the momentum, energy and species equations are modelled by dynamic Smagorinsky or eddy-diffusivity type models [11], based on the generalized Germano identity [12], with six dynamically adjusted coefficients in total. The reaction rate term is modelled by a scale similarity filtered reaction rate model [13].

The droplets are tracked in the Lagrangian frame. The governing equations for every computational droplet are written as

$$\dot{m}_d = \frac{dm_d}{dt} = -\frac{1}{3} \frac{Sh}{Sc} \frac{m_d}{St} H_M \quad (1)$$

$$\frac{dv_{d,i}}{dt} = \frac{F_{drag,i}}{m_d} = \frac{f}{St} (u_{g,i} - v_{d,i}) \quad (2)$$

$$\frac{dT_d}{dt} = \frac{1}{3St} \left[\frac{Nu}{Pr} (T_g - T_d) - (\gamma - 1) Ma^2 \frac{Sh}{Sc} H_M h_{fg} \right] \quad (3)$$

where m_d , $v_{d,i}$, T_d are the mass, i th component of velocity and temperature of the droplets; $u_{g,i}$ and T_g the i th component of velocity and temperature of the gas phase at the droplet location; Sh , Sc , Nu , Pr , Ma , St the Sherwood,

Schmidt, Nusselt, Prandtl, Mach and Stokes numbers; γ the ratio of specific heats; f a correction coefficient to Stokes drag; $F_{drag,i}$ the Stokes drag force exerted on the droplets; H_M the driving potential for mass transfer; h_{fg} the latent heat of evaporation. To simplify the analysis, the gravity force on both phases is neglected. The source terms contributed by droplets that appear in the gas phase governing equations are

$$S_{ms} = -\frac{1}{V} \sum_k \dot{m}_{d,k} \quad (4)$$

$$S_{mo,i} = -\frac{1}{V} \sum_k (F_{drag,k,i} + \dot{m}_{d,k} v_{d,k,i}) \quad (5)$$

$$S_{en} = -\frac{1}{V} \sum_k \left[\frac{1}{3} \frac{Nu}{(\gamma-1)Ma^2 Pr} \frac{m_{d,k}}{St_k} (T_{g,k} - T_{d,k}) + \frac{1}{(\gamma-1)Ma^2} \dot{m}_{d,k} T_{d,k} + \dot{m}_{d,k} h_{fg} + F_{drag,k,i} v_{d,k,i} + \frac{1}{2} \dot{m}_{d,k} v_{d,k,i} v_{d,k,i} \right] \quad (6)$$

where S_{ms} , $S_{mo,i}$, S_{en} are the source terms on the right-hand-side of mass, momentum and energy equations (refer to [10] for the gas phase equations). V is the filtering volume in LES. S_{ms} appear in the species equation for Y_v as well.

Detailed information of numerical methods for the gas phase, including spatial/time discretization schemes and initial/boundary conditions, can be found in [10]. A semi-analytical scheme [14] is used for droplet marching. A 4th-order Lagrangian interpolation scheme [15] is utilized to obtain gas properties at droplet locations.

A 3D free turbulent reactive planar jet laden with non-reactive evaporating liquid droplets has been simulated under different conditions shown in Table 1. Figure 1 presents the schematic of the computational domain and the boundary conditions are described in [10]. The domain size is chosen as $L_x \times L_y \times L_z = 8 \times 31.8 \times 42.785$, where the subscripts x , y and z designate the spanwise (periodic), lateral and streamwise direction, respectively. The sponge layer [10] starts at $z=40$. A uniform grid system $n_x \times n_y \times n_z = 41 \times 160 \times 200$ leads to grid spacing $\Delta x \times \Delta y \times \Delta z = 0.2 \times 0.2 \times 0.215$. Droplets enter the computational domain with the fuel jet through the slot nozzle after $t=20$, when the jet flame has been ignited and established in downstream regions. When a droplet leaves one end of the periodic boundary, a new one with identical properties as the leaving one is put at the corresponding position at the other end.

RESULTS AND DISCUSSIONS

As part of the validation procedure, our LES results of a 3D non-reactive transitional hot jet compared well with the experimental data in [16]. The main simulation parameters taken from [16] are $Re=4000$ and $S=0.76$, where S is the density ratio of hot fuel to environmental air at the inflow plane. In the present reacting jet, the combustion parameters are $Da=3$, $Ze=12$, $T_f=4$ and $Q_h=250$, where Da is Damköhler number, Ze Zeldovich number, T_f adiabatic flame temperature, Q_h heat of combustion, all defined in [10]. In Table 1, St_0 is the initial Stokes number of drop-

lets, designating the normalized initial droplet size, and MLR is the mass loading ratio, defined as the ratio of mass flow rate of droplets to that of the hot fuel at the slot nozzle exit. Figure 1 shows the isosurface of vorticity magnitude, 0.25, at $t=100$ for Case A, a pure reacting jet. The flow field develops from a laminar flow at the inflow, forming large scale vortices at $z \approx 10$, and subsequently breaking up into small scale structures at $z \approx 20$.

Table 1: Simulation Cases

Cases	St_0	MLR
A	-	0
B	1	0.1
C	16	0.1
D	16	1.7

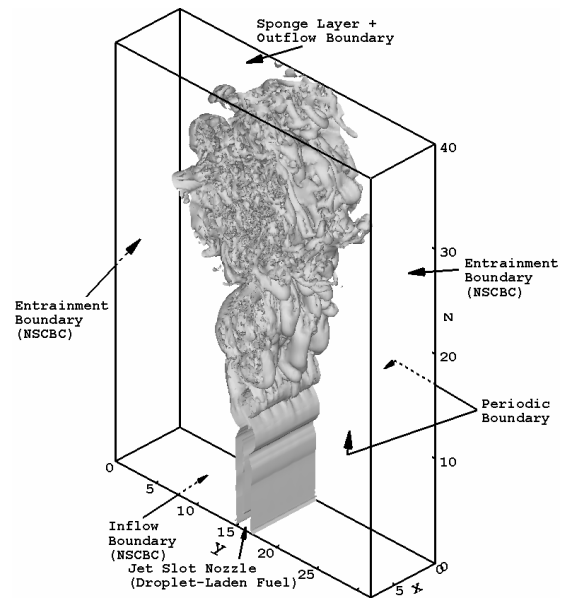


Figure 1: Schematic of the computational domain, boundary setup and the isosurface of vorticity magnitude (0.25) of Case A at $t=100$.

1. Diluted Combustion

A comparison of the averaged temperature fields at $t=100$ for all cases is shown in Fig. 2. At small MLR (0.1), the fields of droplet Cases B and C are very similar to that in Case A without droplets, in terms of the first vortex roll-up, break-down location and spreading rate, etc. However, Cases B and C have dramatically different effects on combustion and consequently peak temperature due to different droplet sizes. The deployment of more droplets while keeping the droplet size the same results in further suppression, as seen in Figs. 2c and 2d for the $St_0=16$ cases. Since the peak temperature in Case D is almost equal to the initial hot fuel temperature, combustion has been fully suppressed. Meanwhile, the lateral spreading of the jet and droplets becomes much less than in other cases, due to the lack of expansion of the mixture of hot reaction products.

Figure 3 presents the profiles of normalized temperature fluctuation intensities for all cases at selected loca-

tions. The peak intensity values for Case A appear in the strong reacting area ($z > 30$), with T_{rms} reaching almost 25% of the mean temperature. In all droplet cases, the temperature fluctuation intensity is dramatically reduced, especially in Case D, due to the cooling effects of droplets and lack of combustion-induced temperature fluctuations. In the near field (close to nozzle exit), droplets play a role as external disturbances on the laminar flow, which lead to higher level of flow fluctuations (not plotted) and in some locations larger temperature fluctuations. Figure 3b shows that high values of temperature fluctuation intensity are usually distributed at the interface between the fuel and the oxidizer ambient, where there is strong combustion, similar to the double peak distribution widely observed experimentally.

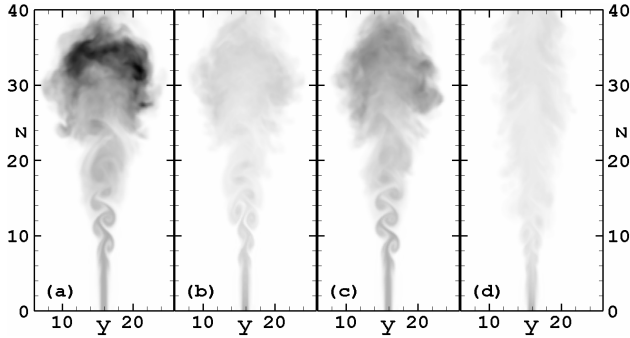


Figure 2: The temperature fields averaged over the periodic spanwise direction at $t=100$ for (a) Case A, (b) Case B, (c) Case C and (d) Case D. A same legend (1-2.087) is used for all the contour plots. The peak temperature in the whole domain for (a), (b), (c) and (d) is 3.12, 1.39, 2.17 and 1.32, respectively.

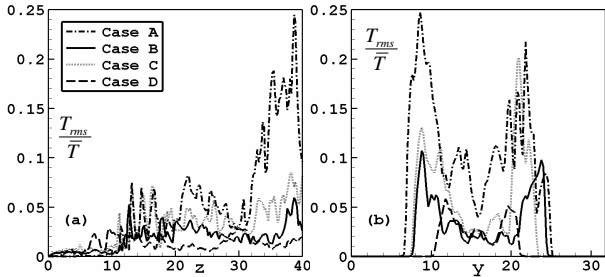


Figure 3: The normalized temperature fluctuation intensities $t=100$: (a) streamwise profile along the jet centreline; (b) lateral profile at $z=30$.

Figure 4 presents some key parameters for Cases A and D to illustrate the effects of combustion and droplets on flow. In Fig. 4a, the mass fraction of vapour, Y_v is considerable, due to effects of combustion at an earlier time or more upstream locations. However, once vapour is produced, the cooling effect of evaporation suppresses the reaction rate (RR). As a result, the RR in Case D is very low compared with that in Case A, as if it were a non-reacting jet. The turbulent kinetic energy (TKE) is found to be higher in Case D than in Case A for most downstream locations. In the non-reacting cases in [17], it was found that “small particles tend to attenuate the turbulence while larger particles augment the turbulence level”. In the present reacting jet, an additional factor is that combustion-induced high temperature will increase molecular

viscosity, which decreases TKE. Also shown in Fig. 4c is the vorticity magnitude ($|\omega|$), which is defined as the square root of the enstrophy, measuring the stretching and tilting, an important mechanism for turbulence production. Consistent with the trend in TKE, the peak magnitude of $|\omega|$ is higher in the droplet case.

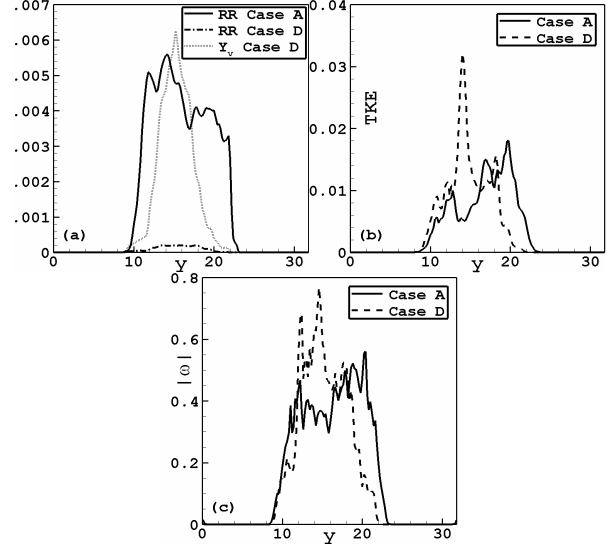


Figure 4: Averaged profiles of key parameters at $z=34$ and $t=100$. (a) Reaction Rate (RR) and mass fraction of vapour (Y_v); (b) Turbulent Kinetic Energy (TKE); (c) Vorticity magnitude.

2. Droplet Dynamics

In Figs. 5a and 5b, the droplet distributions are shown for Cases B and C. In Case B at the transitional region, the small ($St_0=1$) droplets follow the flow and concentrate in the circumferential regions of large scale vortices or high-strain-rate regions, due to their tendency for “preferential concentration” [18]. These are the regions where chemical reactions are strong thanks to better mixing of the fuel and oxidizer. The concentration of droplets there not only reduces the temperature through evaporation, but also separates the fuel from the oxidizer, leading to effective suppression of combustion and thus peak temperature. In the turbulent region downstream, the droplet size becomes even smaller on average, resulting in even more rapid evaporation and effective suppression of combustion, as seen in Fig. 6b, which shows the Probability Density Function (PDF) profiles of the normalized droplet sizes at two heights, i.e., $Z1 = 10 \pm 1$ and $Z2 = 30 \pm 1$, the typical transitional and turbulent regions. The PDF at $Z2$ shows that the droplets are smaller and have a wider spread of sizes than those at $Z1$. For the PDFs calculated with all the droplets in the whole domain at $t=100$, Fig. 6a shows that the initially large droplets (Cases C and D) have evaporated to a lesser extent than in Case C. This is partly because smaller droplets (with the same MLR) have a larger total surface area, which enhances heat transfer and evaporation. Another reason is that larger droplets are less responsive to the flow field and less likely to concentrate in the regions with strong combustion and thus high temperature. Also shown in Fig. 6a is that increasing MLR inhibits evaporation of individual droplets, comparing the

PDFs of Cases C and D. However, the total mass of the vapour produced in Case D is much more than in Case C (not shown), due to 13 times more droplets existing in the whole domain of Case D than in Case C at $t=100$. This leads to the different degree of reaction suppression in these two cases, as seen in Figs. 2c and 2d.

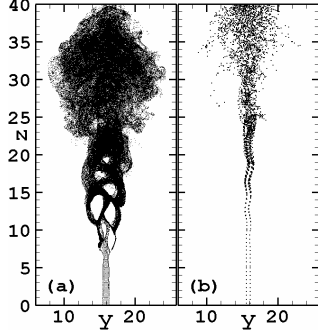


Figure 5: The instantaneous droplet distribution at $t=100$ for (a) Case B and (b) Case C.

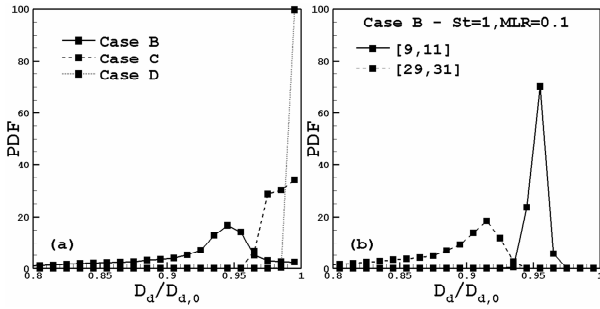


Figure 6: The PDF profiles of the normalized droplet sizes.

The effects of droplets with different initial sizes on the flow field can be scrutinized via the analysis of the grid-scale (GS) kinetic energy budget, which can be written as

$$\frac{D\hat{k}}{Dt} = \underbrace{-\widetilde{u_{g,k}} \frac{\partial \bar{p}}{\partial x_k}}_{\text{I}} + \underbrace{\frac{\partial (\widetilde{\sigma_{ik} u_{g,i}})}{\partial x_k}}_{\text{II}} - \underbrace{\widetilde{\sigma_{ik}} \frac{\partial \widetilde{u_{g,i}}}{\partial x_k}}_{\text{III}} - \underbrace{\frac{\partial (\widetilde{\rho_g \tau_{ik} u_{g,i}})}{\partial x_k}}_{\text{IV}} \quad (7)$$

$$+ \underbrace{\widetilde{\rho_g \tau_{ik}} \frac{\partial \widetilde{u_{g,i}}}{\partial x_k}}_{\text{V}} - \underbrace{\frac{\widetilde{u_{g,i} u_{g,i}}}{2} S_{ms}}_{\text{VI}} + \underbrace{\widetilde{u_{g,i} S_{mo,i}}}_{\text{VII}}$$

The operators, “ \sim ”, “ $\bar{\cdot}$ ” and “ $\hat{\cdot}$ ”, designate the Favre filtering, normal filtering and those functions evaluated using filtered variables, respectively. \hat{k} is the grid-scale kinetic energy (GSKE), representing the large-scale flow structure behaviour and playing a key role in entrainment and turbulent mixing, $\hat{k} = \overline{\rho_g \widetilde{u_{g,i} u_{g,i}}}/2$; \bar{p} is the filtered thermodynamic pressure; $\widetilde{\sigma_{ij}}$ is the shear stress tensor; τ_{ij} is the SGS stress tensor, $\tau_{ij} = \overline{u_{g,i} u_{g,j}} - \widetilde{u_{g,i} u_{g,j}}$. In Eq. (7), term I represents the convection of pressure waves, II the viscous diffusion, III the viscous dissipation, IV the redistributive effect due to interactions between SGS stresses and velocities, V the SGS dissipation, VI the SGS effect of droplets due to evaporation, and VII the SGS effect of droplets due to momentum exchange between the two phases.

Figure 7 presents the contributions of the dominant terms (I, IV, V and VII) in Eq. (7) for all the droplet cases at $z=30$ and $t=100$. In all the cases, combustion-generated pressure gradients due to local thermal expansion lead to the dominance of term I. For a well-resolved LES, the magnitudes of term III (not shown) should be much smaller than those of term V, which has been correctly captured in all the cases, indicating a proper choice of the grid spacing in the current LES. Moreover, the effect of SGS redistribution of GSKE (term IV) has been found to be much more efficient than the GS redistribution effect (term II), which is consistent with the findings in [19]. Since $\overline{S_{ms}} > 0$, VI always acts as a “sink” and tends to decrease the GSKE. However, its magnitude has been found to be too small to trigger any profound effect on GSKE in all the cases presented here. The droplet term due to momentum exchange (VII) plays different roles depending on the droplet initial sizes, i.e., St_0 . For Case B, thanks to the small droplet responsive time, the relative velocities between the flow and droplets are small and the effect of momentum exchange on GSKE is negligible. For the opposite reasons, the droplet momentum effect is more pronounced for Cases C and D. Even with small MLR (0.1), VII has risen to the budget level of the SGS dissipation term V, but is still smaller than the SGS redistribution term IV. In Case D, in which the MLR is much higher, VII becomes the second most important term after the combustion term I. It’s worth noting that VII is basically positive, which acts as a source term for GSKE. Therefore, larger droplets act as a “turbulence promoter”, which could trigger an earlier transition to turbulence as comparison of the different cases in Fig. 2 would reveal. It should be pointed out that the conclusions drawn in this section have been verified at different downstream locations and time instants.

CONCLUSIONS

Large-eddy simulation has been employed to simulate a turbulent reactive jet with and without evaporating droplets to investigate the interactions among turbulence, combustion and evaporating droplets. Dynamic models are employed for all the subgrid terms, except that the filtered reaction rate term is modelled by a scale similarity model, in order to capture the highly local and transient nonlinear interactions. Although a full description of such complex interactions is beyond the scope of a short paper, the present paper has shed light on the different dynamics introduced by droplets of different size and mass loading. Smaller droplets tend to concentrate in high-shear regions where mixing of fuel and oxidizer and consequently combustion predominantly takes place. They are therefore very efficient in suppressing combustion through evaporation of a large number of droplets and by separating fuel from oxidizer. In contrast, bigger droplets are less responsive to the gas phase, and their effect on combustion is less strong. When the droplet size is kept the same, increasing droplet numbers have a larger effect on combustion, as anticipated.

The temperature and intensity of temperature fluctuations are both attenuated when droplets are introduced in

all cases but the extent of attenuation depends on droplet properties. The vorticity magnitude and turbulent kinetic energy in the reactive jet with droplets are generally higher than in the pure reactive jet without droplets, mainly because the reduced temperature field leads to lower viscous dissipation.

The budget analysis on the grid-scale kinetic energy (GSKE) reveals that the droplet evaporation effect on the GSKE is small, and the droplet momentum effect depends on initial droplet sizes (St_0). Unlike the smaller droplets ($St_0=1$), the momentum exchange between the two phases is much stronger for the bigger droplets ($St_0=16$), which can have profound influence on GSKE, and consequently on mixing and entrainment of the flow field, provided that the mass loading ratio is sufficiently high.

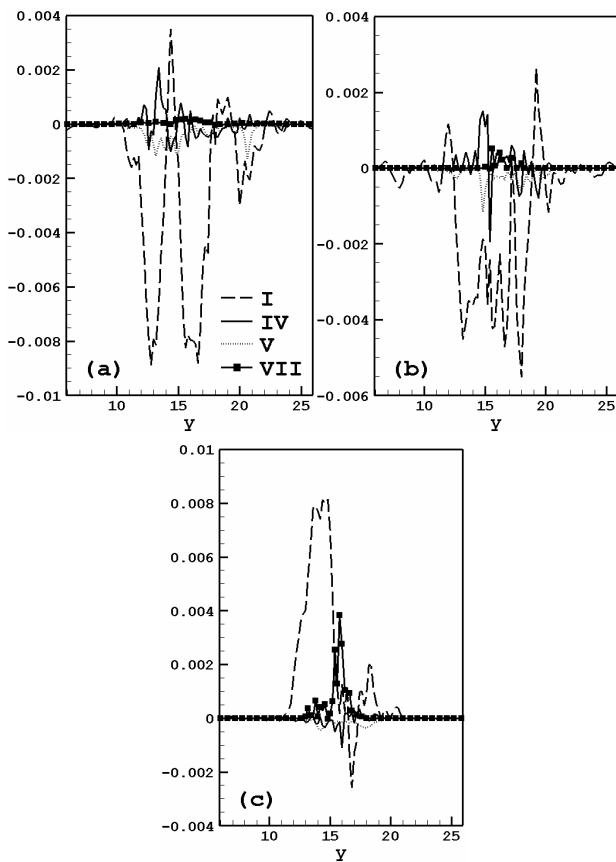


Figure 7: The x -averaged GSKE budget at $z=30$ when $t=100$ for (a) Case B, (b) Case C and (c) Case D.

BIBLIOGRAPHY

[1] Mashayek F. “Droplet-turbulence interactions in low-Mach-number homogeneous shear two-phase flows” *J. Fluid Mech.*, Vol. 367, pp. 163-203, 1998.

[2] Miller R.S. and Bellan J. “Direct numerical simulation of a confined three-dimensional gas mixing layer with one evaporating hydrocarbon-droplet-laden stream” *J. Fluid Mech.*, Vol. 384, pp. 293-338, 1999.

[3] Miller R.S. “Effects of nonreacting solid particle and liquid droplet loading on an exothermic reacting mixing layer” *Phys. Fluids*, Vol. 13, pp. 3303-3320, 2001.

[4] Yuu S., Ueno T. and Umekage T. “Numerical simulation of the high Reynolds number slit nozzle gas-particle

jet using subgrid-scale coupling large eddy simulation” *Chemical Engineering Science*, Vol. 56, pp. 4293-4307, 2001.

[5] Squires K.D. and Eaton J.K. “Particle response and turbulence modification in isotropic turbulence” *Phys. Fluids A*, Vol. 2, pp. 1191-1203, 1990.

[6] Michioka T., Kurose R., Sada K. and Makino H. “Direct numerical simulation of a particle-laden mixing layer with a chemical reaction” *Int. J. Multiphase Flow*, Vol. 31, pp. 843-866, 2005.

[7] Sadiki A., Chrigui M., Janicka J. and Maneshkarimi M.R. “Modelling and simulation of effects of turbulence on vaporization, mixing and combustion of liquid-fuel sprays” *Flow Turbulence Combust.*, Vol. 75, pp. 105-130, 2005.

[8] Janicka J. and Sadiki A. “Large eddy simulation of turbulent combustion systems” *Proc. Combust. Inst.*, Vol. 30, pp. 537-547, 2005.

[9] Boivin M., Simonin O. and Squires K.D. “On the prediction of gas-solid flows with two-way coupling using large eddy simulation” *Phys. Fluids*, Vol. 12, pp. 2080-2090, 2000.

[10] Jiang X. and Luo K.H. “Spatial direct numerical simulation of the large vertical structures in forced plumes” *Flow Turbulence Combust.*, Vol. 64, pp. 43-69, 2000.

[11] Moin P., Squires K., Cabot W. and Lee S. “A dynamic subgrid-scale model for compressible turbulence and scalar transport” *Phys. Fluids A*, Vol. 3, pp. 2746-2757, 1991.

[12] Vreman B. “Direct and large-eddy simulation of the compressible turbulent mixing layer” Ph.D. Thesis, University of Twente, 1995.

[13] DesJardin P.E. and Frankel S.H. “Large eddy simulation of a nonpremixed reacting jet: Application and assessment of subgrid-scale combustion models” *Phys. Fluids*, Vol. 10, pp. 2298-2314, 1998.

[14] Ling W., Chung J.N. and Crowe C.T. “Direct numerical simulation of a two-way thermally coupled droplet-laden mixing layer” *J. Fluid Mech.*, Vol. 437, pp. 45-68, 2001.

[15] Balachandar S. and Maxey M.R. “Methods for evaluating fluid velocities in spectral simulations of turbulence” *J. Comput. Phys.*, Vol. 83, pp. 96-125, 1989.

[16] Yu M.H. and Monkewitz P.A. “Oscillations in the near field of a heated two-dimensional jet” *J. Fluid Mech.*, Vol. 255, pp. 323-347, 1993.

[17] Crowe C., Sommerfeld M. and Tsuji Y. “Multiphase flows with droplets and particles” CRC Press, London, 1998.

[18] Squires K.D. and Eaton J.K. “Preferential concentration of particles by turbulence” *Phys. Fluids A*, Vol. 3, pp. 1169-1179, 1991.

[19] da Silva C.B. and Métais O. “On the influence of coherent structures upon interscale interactions in turbulent plane jets” *J. Fluid Mech.*, Vol. 473, pp. 103-145, 2002.